phys. stat. sol. (c) 5, No. 7, 2490–2494 (2008) / DOI 10.1002/pssc.200777634

physica status solidi c
www.pss-c.com
current topics in solid state physics

Polarization sensitive spectroscopy of charged quantum dots

E. Poem[*,1], J. Shemesh[1], I. Marderfeld[1], D. Galushko[1], N. Akopian[1], D. Gershoni[1], B. D. Gerardot[2], A. Badolato[2], and P. M. Petroff[2]

[1] Department of Physics, The Technion - Israel Institute of Technology, Haifa 32000, Israel
[2] Materials Department, University of California Santa Barbara, CA 93106, USA

Received 10 September 2007, revised 25 September 2007, accepted 3 December 2007
Published online 22 February 2008

PACS 73.21.La, 78.55.-m, 78.67.Hc

[*] Corresponding author: e-mail poem@tx.technioc.ac.il, Phone: +972 4 829 3923, Fax: +972 4 823 5107

We present an experimental and theoretical study of the polarized PL spectrum of single semiconductor quantum dots in various charge states. We compare our polarization sensitive spectral measurements with a novel many-carrier theoretical model. The model considers both the isotropic and anisotropic exchange interactions between all participating electron-hole pairs. We demonstrate that lines emanating from evenly charged states are linearly polarized. Their measured polarization direction does not necessarily coincide with the traditional crystallographic direction. It depends on the shells of the single carriers which participate in the recombination process.

1 Introduction The photoluminescence (PL) spectrum of single self-assembled semiconductor QDs is usually composed of many discrete spectral lines. The variety of lines originates from optical transitions between various many carrier configurations and different QD charge states [1-3]. Several experimental techniques, such as excitation intensity dependent PL spectroscopy [4] and electro-PL spectroscopy [2, 3] are used for associating a given spectral line with a specific optical transition. Unfortunately, even when these and other methods are combined, occasionally, some lines still remain unidentified. Polarization sensitive PL spectroscopy has also been applied to aid in line identification. Most notably, the neutral exciton and the neutral biexciton lines are split into two cross linearly polarized doublets [5], while singly charged excitonic lines are unpolarized.

In this work we focus our studies on polarization sensitive PL spectroscopy of single semiconductor quantum dots. We carefully measure the polarization of the PL spectra under various excitation conditions. Our results are then compared with, and analyzed by, a novel theoretical many charge-carriers model which is based on the full configuration interaction (FCI) method [6]. The novelty in our model is in its inclusion of the electron-hole exchange interaction (EHEI) [7, 8]. We show that the model provides a very good understanding of the experimental measurements.

2 Experimental

2.1 Sample The sample was grown by molecular beam epitaxy on a [001] oriented GaAs substrate. One layer of strain-induced InGaAs QDs was deposited in the center of a one wavelength planar microcavity (MC) in order to enhance the collection efficiency. The MC was formed by two distributed Bragg reflectors deposited below and above a QD-emission-wavelength wide GaAs spacer. The Q-factor of the MC is about 500. In order to electrically charge the QDs, a p-i-n junction was formed by n (p) -doping the layers below (above) the GaAs spacer, which was left intrinsic. An additional intrinsic AlAs barrier was grown inside the GaAs spacer between the p-type region and the QDs. This barrier prolongs the hole's tunneling time out of the QDs in respect to that of the electron, and enables positive charging. The sample was not patterned or processed laterally to prevent obscuration of the emission and its polarization.

2.2 Optical characterization For the optical measurements we used a diffraction limited low temperature

confocal optical microscope [1]. The collected light was dispersed by a 1 meter monochromator and detected by a cooled CCD array detector. The spectral resolution of the system is 15 μeV. The polarization of the emitted light was analyzed by two computer controlled liquid crystal variable retarders and a linear polarizer in front of the monochromator, in the following manner: Six independent measurements of spectra polarized along the H, V, D, $\bar{D}$, R and L directions (see below) were taken. From these spectra, the Stokes parameters for each pixel were deduced. From these parameters, the polarization vector inside the Poincaré sphere was determined for each pixel.

Throughout this work we use the symbol H (V) for linear light polarization along the [$\bar{1}$10] ([110]) crystallographic axis of the sample. The symbol D ($\bar{D}$) is used for the (cross) diagonal polarization, while the symbol R (L) is used for the right (left) hand circular polarization.

In Fig. 1 we show the PL spectra from a single QD as a function of the voltage applied to the sample. The QD was excited by a cw 1.47 eV Ti-sapphire laser light.

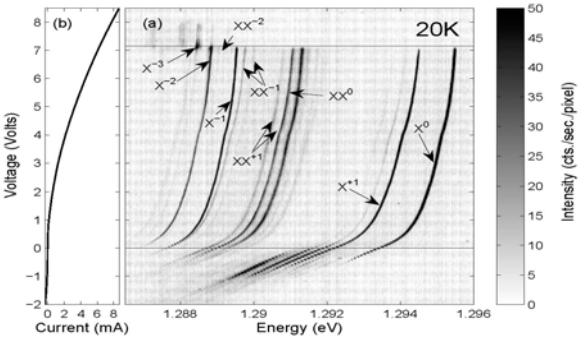

Figure 1 (a) Measured PL spectra from a single SAQD, as a function of the bias on the device. The QD was excited by 1.47 eV cw-light. The various spectral lines are labeled by X (XX) for single (double) initial e-h pair occupation, and a superscript which denote the QD charge state during the recombination. The horizontal solid lines mark the voltages for which spectra are presented in Fig. 2. (b) The current through the device as a function of the bias voltage.

The specific structure of our sample is such that at forward biases (above ~7 volts) the QDs are negatively charged as clearly evident by the abrupt step in the emission energy. This injection induced charging mechanism is similar to that reported earlier [2]. At large reverse biases, however, the QD is increasingly positively charged, due to vast difference between the tunneling-out rates of electrons and holes. The spectral line identification in Fig. 1 is based on the order by which the lines appear and disappear as the voltage on the device increases. Information gained from excitation intensity dependence PL spectroscopy (not shown) and polarization sensitive spectroscopy (see below) is also used for this purpose. In Fig. 2 we present the measured polarization sensitive spectra for the bias voltages indicated by horizontal lines in Fig. 1. In Fig. 2(a), the QD was on average neutral. Spectral lines of a neutral, as well as of a singly negatively and singly positively charged QD are observed. The corresponding polarization spectra projected on the linear H-V and on the linear D-$\bar{D}$ axes of the Poincaré sphere are shown in Fig. 2(b).

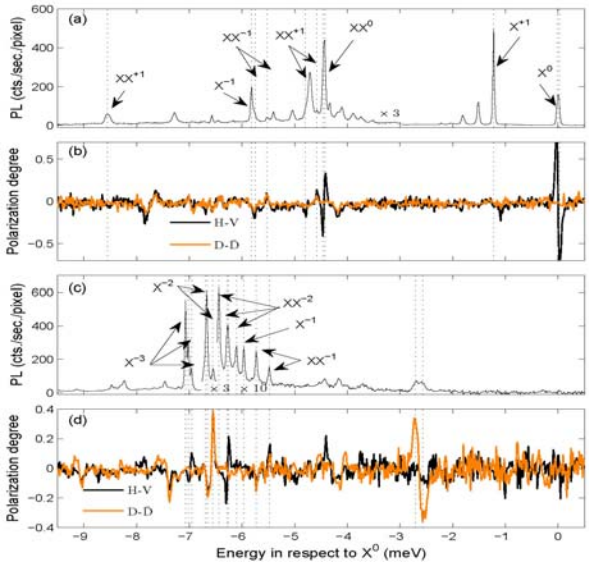

Figure 2 (color online) (a) Measured PL spectrum for bias voltage of 0V. The energy is measured from the energy of the X^0 line. (b) PL polarization spectra for bias voltage of 0 V. The black (orange) lines present the polarization as projected on the H-V (D-$\bar{D}$) axis of the Poincaré sphere. (c) and (d) are the same as (a) and (b) for a bias voltage of 7.15 V.

The projection on the R-L axis was zero to within our experimental uncertainty (not shown).

In Figs. 2(c) and 2(d) we present the PL spectrum and its linear polarization projections, respectively, for a bias voltage of 7.15 V at which the QD was on average, negatively charged with two to three electrons.

We note here that the spectral shapes of the observed negatively charged lines are similar to those observed also in previous works [3, 9].

3 Theoretical model In order to calculate the many-carrier polarized transition spectrum we first solve numerically a single carrier problem for the electron and for the hole in the QD, in the single band, slowly varying envelope function approximation (1-SVEFA). We model the QD potential as a 3D finite well in the shape of a rectangular slab, which long (short) side lies along the H (V) direction. In this manner, we obtain a consistent set of single charge carrier energies and associated wavefunctions. We then use this set in order to construct a many-carrier second quantization Hamiltonian,

$$\hat{H} = \hat{H}_{single} + \hat{H}_{ee} + \hat{H}_{hh} + \hat{H}_{eh} \quad (1)$$

which includes both the single carrier Hamiltonian, and the electrostatic interactions between all confined carriers. We focus now on the electron-hole interaction Hamiltonian,

$$\hat{H}_{eh} = \sum_{\substack{n_1,n_2,n_3,n_4 \\ s_1,s_2,s_3,s_4}} \left(-C^{ehhe}_{\substack{n_1 n_2 n_3 n_4 \\ s_1 s_2 s_3 s_4}} + C^{hehe}_{\substack{n_2 n_1 n_3 n_4 \\ s_2 s_1 s_3 s_4}} \right) \hat{a}^{\dagger}_{n_1,s_1} \hat{b}^{\dagger}_{n_2,s_2} \hat{b}_{n_3,s_3} \hat{a}_{n_4,s_4} \qquad (2)$$

and in particular on the EHEI, which is represented in (2) by the term C^{hehe}. $n_{1..4}$ are indices to the spatial part of the carrier wavefunction, and $s_{1..4}$ are indices to its pseudo-spin part. The pseudo-spin structure of the EHEI for the lowest energy envelope functions is deduced from symmetry considerations (the method of invariants) [7]. The SVEFA requires that the same considerations hold also for any other combination of envelope functions [8]. Thus, we express the electron-hole-exchange terms as follows:

$$C^{hehe}_{\substack{n_2 n_1 n_3 n_4 \\ s_2 s_1 s_3 s_4}} = \begin{pmatrix} \frac{1}{2}\Delta_0^{n_2 n_1 n_3 n_4} & \frac{1}{2}\Delta_1^{n_2 n_1 n_3 n_4} & 0 & 0 \\ \frac{1}{2}\Delta_1^{n_2 n_1 n_3 n_4 *} & \frac{1}{2}\Delta_0^{n_2 n_1 n_3 n_4} & 0 & 0 \\ 0 & 0 & -\frac{1}{2}\Delta_0^{n_2 n_1 n_3 n_4} & \frac{1}{2}\Delta_2^{n_2 n_1 n_3 n_4} \\ 0 & 0 & \frac{1}{2}\Delta_2^{n_2 n_1 n_3 n_4} & -\frac{1}{2}\Delta_0^{n_2 n_1 n_3 n_4} \end{pmatrix} \qquad (3)$$

The e-h pseudo-spin base for the matrix are the functions: $\{|\downarrow\Uparrow\rangle, \ |\uparrow\Downarrow\rangle, \ |\uparrow\Uparrow\rangle, \ |\downarrow\Downarrow\rangle\}$ The terms $\Delta_0^{n_2 n_1 n_3 n_4}$ and $\Delta_2^{n_2 n_1 n_3 n_4}$ are mainly affected by the short range interaction [8]. This intra-unit-cell interaction is not sensitive to the details of the slowly varying envelope wavefunctions [8]. Therefore, we assume that all the non vanishing $\Delta_0^{n_2 n_1 n_3 n_4}$ and $\Delta_2^{n_2 n_1 n_3 n_4}$ have the same values, Δ_0 and Δ_2, respectively. The values that we used were chosen such that the calculated X^0 spectrum would match the magneto-PL measured X^0 spectrum [10]. The $\Delta_1^{n_2 n_1 n_3 n_4}$ terms are mainly affected by the second order terms in the expansion of the long-range interaction [7, 8]. This interaction is very sensitive to the shape of the envelope functions. In order to gain insight and to reduce the needed computation resources, we calculated these terms using the analytical wavefunctions of a 2D elliptic harmonic oscillator, rather than the numerical wavefunctions [11]. For Δ_1^{1111} we obtained,

$$\Delta_1^{1111} = \frac{3\sqrt{\pi} e^2 \hbar^2 E_p (\xi - 1)}{8\varepsilon m_0 E_g^2 \left(l_x^e\right)^3 \xi^2 \beta \sqrt{1+\beta^2}} = -15\mu eV \qquad (4)$$

for electron oscillator major semi-axis l_x^e =72 Å, hole/electron length ratio β=0.72 and minor/major semi-axis ratio (the aspect ratio) ξ=0.96. E_p=25.5 eV is the conduction-valence dipole energy, E_g =1 eV is the band gap, and ε=13.8 is the dielectric constant of the QD material [12]. m_0 is the free electron mass, and e is the electron's charge. l_x^e is extracted from the measured s-p separation [1], β is extracted from the measured energy separation between the positively and negatively charged excitons and ξ is extracted from the ratio of the anisotropic splitting energy of the doubly charged exciton (which approximately equals Δ_1^{1212}) to that of the neutral exciton (which approximately equals Δ_1^{1111}). Table 1 lists the measured EHEI parameters, the analytical ratios of several $\Delta_1^{n_2 n_1 n_3 n_4}$ terms to Δ_1^{1111} and their values obtained using the measured Δ_1^{1111}. The values listed in Table 1 are the values used for the many-carrier calculations. The many body Hamiltonian is diagonalized, and collective many carriers energies and wavefunctions are obtained.

Table 1 Measured and calculated electron-hole exchange interaction terms (in μeV) used for calculating the PL spectra. The ratios, calculated for harmonic oscillator functions, are given in terms of the hole/electron length ratio β and the aspect-ratio ξ for $|1-\xi| << 1$.

Parameter	Used in calculations	Ratio to Δ_1^{1111}
Δ_0	207*	-
Δ_2	21*	-
Δ_1^{1111}	-25*	-
Δ_1^{1212}	196*	$\frac{\beta^2}{1+\beta^2}\frac{2\xi-1}{\xi-1}$
Δ_1^{1313}	-222	$\frac{\beta^2}{1+\beta^2}\frac{\xi-2}{\xi-1}$
Δ_1^{1414}	-6.4	$\frac{\beta^4}{\left(1+\beta^2\right)^2}\frac{41-6\xi}{16}$
Δ_1^{1515}	232	$\frac{1}{2}+\frac{\beta^2}{1+\beta^2}\frac{1}{\xi-1}+\frac{\beta^4}{\left(1+\beta^2\right)^2}\frac{61\xi-45}{32(\xi-1)}$
Δ_1^{2121}	379	$\frac{1}{1+\beta^2}\frac{2\xi-1}{\xi-1}$
Δ_1^{1213}	$209i$	$i\frac{\beta^2}{1+\beta^2}\frac{\xi+1}{2(\xi-1)}$

* Measured.

We then use the dipole approximation to calculate the optical transition amplitudes between the many carriers' states for the 6 polarizations discussed above. From these amplitudes we calculate the Stokes parameters and obtain the polarization state for each transition.

4 Comparison between experimental measurement and model calculations In Fig. 3 we compare the measured and calculated po-larized fine structure of various spectral lines.

We note in Fig. 3 that the measured fine structures are reproduced quite nicely by our model calculations. In particular, the calculated number of fine structure components, their relative intensities and their polarizations correlate with the measured values. On the other hand, while the calculated polarization spectra are always polar-

ized along the H-V axis of the poincaré sphere, the measured ones are sometimes rotated (see below). The calculated energy differences between the components of the X^{-3} line and the calculated splitting between the unpolarized and polarized doublets of the X^{-2} line are larger than the measured ones. We believe that this may be a consequence of the dependencies of Δ_0 on the envelope wavefunctions, which are neglected in our model.

In non-resonant excitation, and in the absence of magnetic field, the theory predicts that the spectral lines can only present linear polarizations. This is what we observed experimentally as well. In the theoretical model, the linear polarization can only be oriented along the main axes of the QD, i.e. along H and V. In the experiment, however, we found that the polarization appears in *three* sets of orthogonal axes: The measured polarization of the neutral exciton line is indeed along the H-V axis of the Poincaré sphere. A few other lines, most notably the neutral biexciton, are also polarized along this axis.

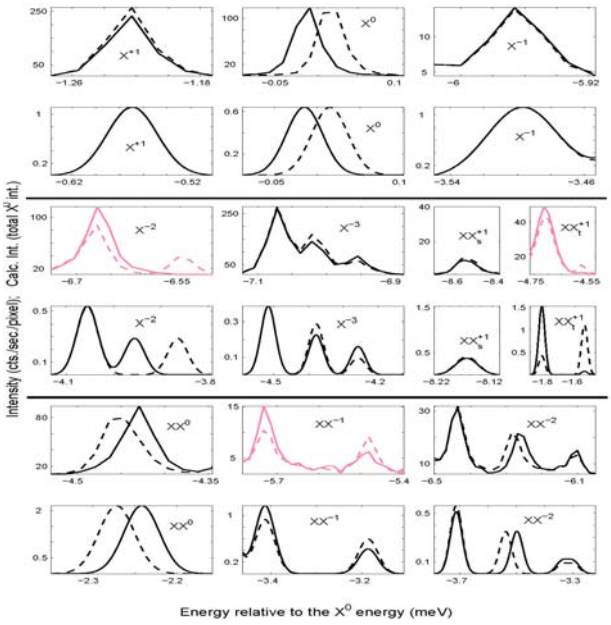

Figure 3 Measured (top panel in each pair) and calculated (bottom panels) high resolution polarization sensitive PL spectra of various spectral lines. The solid (dashed) black line represents H (V) polarized spectrum while the solid (dashed) pink line represents the V+ $\bar{D}$ (H+D) polarized spectrum.

Few other spectral lines are polarized along an axis which is rotated clockwise by 135 degrees relative to the H-V axis of the Poincaré sphere. This polarization axis, which roughly coincides with the [$\bar{1}$ 20] and the [210] directions, appears only in lines associated with configurations which contain one unpaired p_x carrier. For other configurations, which contain only *s* carriers or either closed shells or two unpaired *p* carriers (p_x and p_y), the polarization is along the H-V axis. In addition, we sometimes observe lines which are polarized along the D- $\bar{D}$ axis as well. Such a spectral line is seen in Fig. 3(d), at energy of -2.6 meV relative to the X^0 line. This relatively weak doublet may result from pair recombination in doubly negatively charged QD as deduced from its voltage dependence.

These novel experimental observations are not reproduced by our theoretical, single band based model, since the model ignores the underlying crystal. In particular, the vectorial nature of the hole Bloch functions is overlooked. Correct inclusion of this nature e.g. by a multi band model, would have resulted in polarized optical transitions to the *p*-shell states, even without the EHEI. We believe that the combined effect of Bloch function's related polarization and EHEI related polarization is the cause for the change of polarization direction.

A multi band model is absolutely necessary for calculating the polarization selection rules in highly positively charged QDs. There, the complicated nature of the *p*-shell holes is not likely to be captured by a one band model. The polarization degree of the highly positively charged QD emission lines (identified by their voltage dependencies) that we measured was marginal, while our single band model yields polarizations similar to those of the negatively charged QD lines. We believe that this discrepancy results from the inadequacy of the single band model [9]. Additionally, we note that the highly positively charged QD lines were all measured under large electrostatic fields, which for now, were not considered in our model.

5 Conclusion We presented detailed polarization sensitive spectroscopy of a single QD in various charge states. We developed a many-carrier model based on single band envelope function approximation, which includes the isotropic and anisotropic electron-hole exchange interactions, for the analysis of the measured data. We calculated the PL spectrum with its fine structure and polarizations for the exciton and biexciton optical transitions in neutral, singly positively and singly, doubly and triply negatively charged QDs. The calculations are favorably compared with the measured polarization sensitive PL spectra. The experimental data display, however, polarizations directions oriented along other directions than the main axes of the QD, when carriers occupy the *p* shells. This indicates, that a one band based model is too simple to describe this novel observation.

Acknowledgements The research was supported by the US-Israel Binational Science Foundation (BSF), the Israeli Science Foundation (ISF) and the Russell Berrie Nanotechnology Institute (RBNI) in the Technion. We thank E. L. Ivchenko for fruitful correspondence.

References

[1] E. Dekel, D. Gershoni, E. Ehrenfreund et al., Phys. Rev. B **61**, 11009 (2000).
[2] R. J.Warburton, C. Schaflein, D. Haft et al., Nature **405**, 926 (2000).

[3] B. Urbaszeck, R. J. Warburton, K. Karrai et al., Phys. Rev. Lett. **90**, 247403 (2003).
[4] D. V. Regelman, U. Mizrahi, D. Gershoni et al., Phys. Rev. Lett. **87**, 257401 (2001).
[5] D. Gammon, E. S. Snow, B. V. Shanabrook et al., Phys. Rev. Lett. **76**, 3005 (1996).
[6] A. Barenco and M. A. Dupertuis, Phys. Rev. B **52**, 766 (1995).
[7] E. L. Ivchenko, G. E. Pikus, Springer Ser. Solid State Sciences, Vol. 110 (Springer Verlag, 1997).
[8] T. Takagahara, Phys. Rev. B **62**, 16840 (2000).
[9] M. Ediger, G. Bester, B. D. Gerardot et al., Phys. Rev. Lett. **98**, 036808 (2007).
[10] S. Alon-Braitbart, E. Poem, L. Fradkin et al., Physica E **32**, 127 (2006).
[11] M. M. Glazov, E. L. Ivchenko, L. Besombes et al., Phys. Rev. B **75**, 205313 (2007).
[12] O. Madelung, M. Schulz, and H. Weiss (Eds.), Landolt-Börnstein, Vol. 17a (Berlin, 1982).

